Radiation Response of AlGaN-Channel HEMTs

M. J. Martinez, *Senior Member, IEEE*, M. P. King, *Member, IEEE*, A. G. Baca, A. A. Allerman, A. A. Armstrong, B. A. Klein, E. A. Douglas, *Member, IEEE*, R. J. Kaplar, *Senior Member, IEEE*, and S. E. Swanson

***Abstract*:We present heavy ion and proton data on AlGaN high-voltage HEMTs showing Single Event Burnout, Total Ionizing Dose, and Displacement Damage responses. These are the first such data for materials of this type. Two different designs of the epitaxial structure were tested for Single Event Burnout (SEB). The default layout design showed burnout voltages that decreased rapidly with increasing LET, falling to about 25% of nominal breakdown voltage for ions with LET of about 34 MeV·cm²/mg for both structures. Samples of the device structure with lower AlN content were tested with varying gate-drain spacing and revealed an improved robustness to heavy ions, resulting in burnout voltages that did not decrease up to at least 33.9 MeV·cm²/mg. Failure analysis showed there was consistently a point, location random, where gate and drain had been shorted. Oscilloscope traces of terminal voltages and currents during burnout events lend support to the hypothesis that burnout events begin with a heavy ion strike in the vulnerable region between gate and drain. This subsequently initiates a cascade of events resulting in damage that is largely manifested elsewhere in the device. This hypothesis also suggests a path for greatly improving the susceptibility to SEB as development of this technology goes forward. Testing with 2.5 MeV protons showed only minor changes in device characteristics.**

***Index Terms*—Aluminum Gallium Nitride (AlGaN), Aluminum Nitride (AlN), burnout, displacement damage (DD), heavy ion, HEMT, High Electron Mobility Transistor, failure analysis, Gallium Nitride (GaN), heavy ions, heavy ion testing, power, proton, radiation effects, radiation effects in devices, radiation-hardness assurance, radiation-hardness assurance testing, semiconductor device breakdown, semiconductor device radiation effects, silicon, single-event burnout (SEB), single-event effects (SEEs), Total Ionizing Dose (TID).**

I. Introduction

GAN microwave transistors (typically High Electron Mobility Transistors, HEMTs) have been studied for some time, and, consequently, have had a fair amount of scrutiny of their response to radiation for space environments [1-4]. There is growing interest in next generation AlGaN-channel based power transistors for power conversion [5-7], which requires higher operating voltages and different operating modes. These devices are attractive for improving size, weight, and power for space applications.

While most work on GaN microwave transistors [1,2] has shown little issue with Single Event Effects (SEE), Total Ionizing Dose (TID), or Displacement Damage (DD), there is little reason to believe that devices designed for high-voltage power conversion would not have at least some of the same issues seen in power Si transistors [8]. Indeed, some recent work on AlGaN/GaN HEMTs for power applications [3,4] has shown a susceptibility to Single Event Burnout (SEB) and related failure mechanisms involving the substrate [4]. Further, to achieve the operating characteristics desirable for power conversion (particularly higher breakdown voltage, BV_{DS}), changes in design and materials make the results seen for GaN HEMTs less applicable to these newer wide-bandgap power devices.

In this work, we investigate Single Event Burnout (SEB), TID, and DD effects in HEMTs that use $Al_xGa_{1-x}N$ with differing concentrations of AlN in both channel and barrier layers with BV_{DS} between 200 V and 500 V. To our knowledge this is the first such testing of this type of device for the space environment.

II. Experimental Details

For this work, two prototypes of $Al_xGa_{1-x}N$ HEMTs were used, with maximum breakdown voltages of 200 V and 500 V, respectively (at a gate-drain spacing of 5 um) [5,6]. They differ in the design of the barrier and channel layers, particularly in the composition of the materials used. They are described in detail in [5,6]. The nominal 200 V device is called "Type I" which has the barrier layer of $Al_{0.45}Ga_{0.55}N$, while the channel layer is $Al_{0.3}Ga_{0.7}N$. The nominal 500 V device is called "Type II" and has the barrier layer of $Al_{0.85}Ga_{0.15}N$, while the channel layer is $Al_{0.7}Ga_{0.3}N$. The substrate in both types is sapphire [5,6], and interface defects are believed to be well isolated by the AlN buffer and not to participate in the types of effects described here. These two device types are shown schematically in Fig. 1. A limited number of research prototypes were available and were not screened for pre-irradiation breakdown voltages, to avoid damaging them.

The prototypes had 20 fingers, with a width of 300 µm each, for a total of 6 mm, a gate length of 2 µm, and varying Gate-Drain (G-D) spacing (5 µm spacing is baseline). An example device is shown in Fig. 2.

Manuscript received July 13, 2018. This work was supported by the Laboratory Directed Research and Development program at Sandia National Laboratories. Sandia National Laboratories is a multimission laboratory managed and operated by National Technology and Engineering Solutions of Sandia, LLC., a wholly owned subsidiary of Honeywell International, Inc., for the U.S. Department of Energy's National Nuclear Security Administration under contract DE-NA-0003525. This paper describes objective technical results and analysis. Any subjective views or opinions that might be expressed in the paper do not necessarily represent the views of the U.S. Department of Energy or the United States Government.

All authors are with Sandia National Laboratories, Albuquerque, NM 87123 USA (email: mmarti8@sandia.gov).

This article has been accepted for publication in a future issue of this journal, but has not been fully edited. Content may change prior to final publication. Citation information: DOI 10.1109/TNS.2018.2885526, IEEE Transactions on Nuclear Science

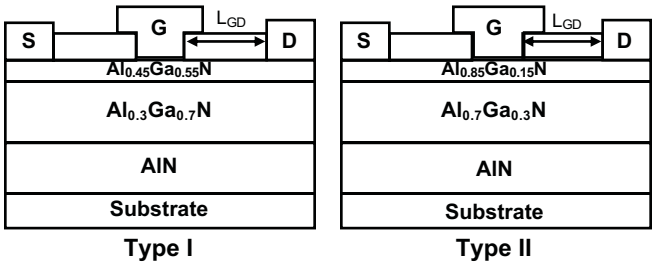

Fig. 1: Schematic cross-section of the two basic device types. Left and right devices are referred to as Type I and Type II, respectively, to distinguish the differing Al concentrations in the barrier and channel layers. The gate-drain spacing, L_{GD} is also shown. Substrate is sapphire for both types.

These devices were packaged in ceramic DIPs with removable lids to allow exposure of the devices to heavy ions. These packages were used with a ZIF-socketed generic test board. A current probe and a high-voltage bias tee were used to measure transient currents and voltages on the drain with high-speed oscilloscopes (time resolution of 100 ps). Since the high-voltage power supplies can only supply low currents, drain connections used capacitors to provide transient current as shown in Fig. 3, below.

Heavy ion testing was conducted at the Tandem Van de Graff facility at Brookhaven National Laboratory, Upton, NY. This type of accelerator facility requires that the Device Under Test (DUT) be placed in a vacuum chamber. Prior to choosing this facility for testing, simulation of the full stack of device materials in SRIM [9] was used to confirm that even in the worst case, heavy ions had little change in Linear Energy Transfer (LET) at ranges well beyond the active layers.

Transistor gates were consistently biased at −6 V to ensure that the channel was pinched off, with one exception. One device had a lower threshold voltage than the others, and was given a gate bias of −10 V, and it behaved similarly to the other devices as far as SEB is concerned.

For these devices, there were two different die types that were packaged. One type had four transistors of the same layout, while the other type had variations in gate-drain spacing (4 µm, 8 µm, and 10 µm) that gave different breakdown voltages.

The experimental plan was to map out the safe operating area (SOA) of drain voltage in the off-state (the most vulnerable operating mode [8]) for ions up to Au (LET=64.7 MeV · cm^2/mg), to get a first estimate of how much voltage derating would be necessary for reliable operation in space radiation environments. In practical terms, this meant starting at low LET and working up to higher LETs, looking for when the ions begin to degrade performance. The exception to this was that, at the beginning, the highest LET was used on one part to confirm that we would see degradation in these devices, since this is a new materials system. Once confirmed, we started with a low-LET ion and start working up to higher LETs.

Most exposures were done to a fluence of 2.5×10^7 ions/cm^2 (0.25 ions/μm^2). Given the dimensions of the transistor active areas, the entire device will have been struck by more than 3×10^4 ions, on average. For the amount of repetition and symmetry in the design, this was deemed more than adequate, as each equivalent spot would have received many ion strikes in a given exposure.

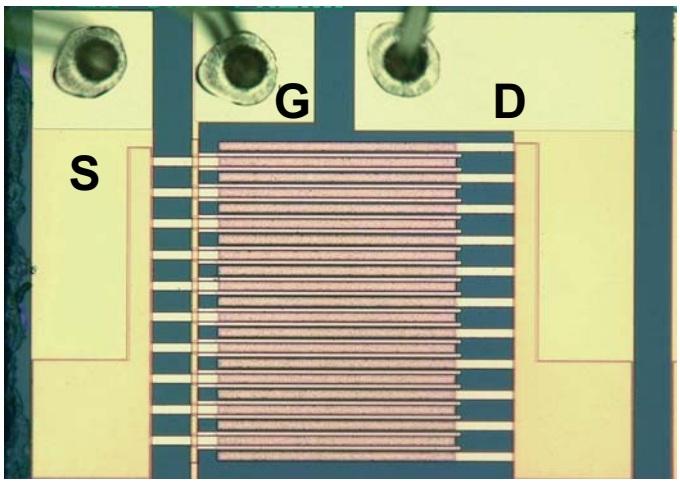

Fig. 2 Example photomicrograph of an $Al_xGa_{1-x}N$-based HEMT.

III. Experimental Results and Discussion

A. *Single Event Burnout as a Function of LET*

To analyze the data, it was necessary to calculate the LET by running simulations in SRIM-2012 [9], which included metal layers, silicon nitride, and the epitaxial layers. Overlayers were the same for the two device types, but LET varies with layer composition, and the value used was that for the channel layer for each of the designs. A summary of the ions, their LETs in $Al_xGa_{1-x}N$, and their ranges is shown in Table I, with LET values given at the top of the channel layer. Note that the LET is higher for the Type II, due to its lower density. Ranges were calculated using the Type I layers, as they are the worst case, having a maximum semiconductor thickness of about 5.7 µm, including the AlN buffer layer, but they are shown as the distance beyond the bottom of the channel, into the buffer and beyond.

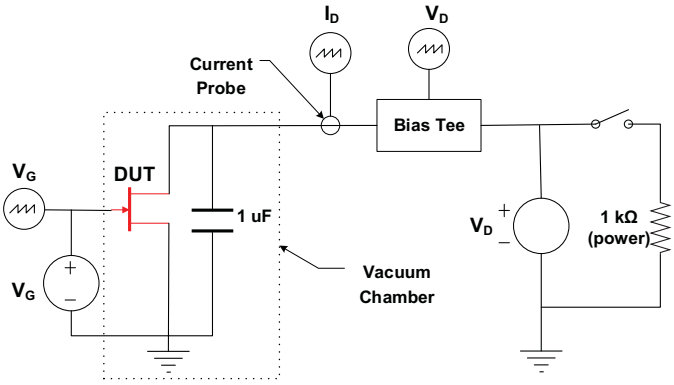

Fig. 3: Schematic of DUT test fixture. The relay switch on the right was for safely discharging the hold-up capacitor after external bias is removed.

This article has been accepted for publication in a future issue of this journal, but has not been fully edited. Content may change prior to final publication. Citation information: DOI 10.1109/TNS.2018.2885526, IEEE Transactions on Nuclear Science

TABLE I: ION SPECIES WITH INCIDENT ENERGIES, CALCULATED LETS, AND CALCULATED RANGES

Ion	Energy (MeV)	LET (MeV−cm²/mg) $Al_{0.3}Ga_{0.7}N$	LET (MeV−cm²/mg) $Al_{0.7}Ga_{0.3}N$	Range† (μm)
F	141	2.95		64
Si	185	6.59	7.28	42
Ti	195	17.4	19.5	22
Fe	232	21.6	24.3	22
Ge	256	29.9	33.6	20
Br	279	33.9		20
Au	303	64.7		15

†All ranges were calculated using the worst case for overlayers, which was the Type I layers, inclusive of all the layers above the substrate, (metals, semiconductors, and dielectrics), irrespective of actual device type.

Because we increased drain voltage in discrete steps, and SEB is a one-time event, we couldn't know the actual threshold voltage to achieve SEB (V_{SEB}). Therefore, we have taken the midpoint between the voltage at which SEB happened and the previous voltage where it did not as an estimate of V_{SEB}, and have used the two voltages as the range for error bars. (For example, if a device passed at 150 V, but failed at the next step at 160 V, it would be shown as 155 V ± 5 V.) It should also be noted that a few of these prototype transistors burned out from simple applied voltage, rather than from radiation, because the devices had to be biased at higher voltages to see SEB for low LETs, bringing us to their BV_{DS}. These are shown and noted for the sake of comparison. In general, nominal breakdown voltages seemed to be about what was expected (~200 V and ~500 V, respectively) for the two designs with 5 μm G-D spacing.

The first set of data to examine is for Type I with the baseline 5 μm G-D layout, plotted in Fig. 4. For ions up to and including Si (LET= 6.59 MeV·cm²/mg), SEB was observed, but generally only very close to the expected BV_{DS} (~200 V). For Ti and heavier ions (LET ≥ 17.4 MeV·cm²/mg), SEB was triggered well below the expected BV_{DS}. In the case of Br (33.9 MeV·cm²/mg), V_{SEB} was only about 25% of expected BV_{DS}, and probably would have been worse for heavier ions, given the observed trend. Also of note is the response to Fe ions (21.6 MeV·cm²/mg), which shows V_{SEB} at slightly higher than 50% of expected BV_{DS}, which is significant because ions heavier than Fe are far less prevalent in the galactic cosmic ray background in space [9], so margin against Fe is often a key metric for shorter space missions. (Fe LET in these tests was within 10% of the peak LET for Fe in these materials.) The Ge (29.9 MeV·cm²/mg) result is also noteworthy because it has an LET similar to that for Ga, which would be one of the common secondary ions for any $Al_xGa_{1-x}N$ device in an energetic proton environment, such as the lower radiation belts. The low V_{SEB} from Ge implies that a significant reduction of the non-rad SOA would be needed in such an environment.

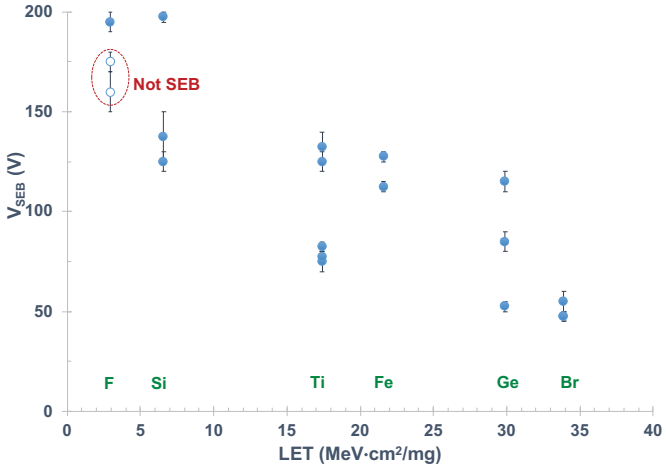

Fig. 4: Plot of the minimum voltage for SEB for 200 V, Type I HEMTs (G-D spacing of 5 μm) versus LET of the incident ions in the channel. The ion species are shown above their respective LETs for clarity. Two devices which failed for non-SEB breakdown are labeled as such and are shown as unfilled points. Error bars not visible are smaller than marker. Each marker represents a single device, and all data are for normal incidence, with a test fluence of 2.5×10^7 ions/cm².

Process stability improvements are still under development, and without screening for actual BV_{DS}, there was more apparent variation in breakdown than we would have liked. For example, when testing with F ions, some devices broke down (from bias increase while not being exposed to any ions) well below 200 V, while others could be biased to 200 V without breakdown, and, this likely leads to some variability in measured V_{SEB}. This is a situation that complicates interpretation, but which will improve as the technology matures. What is clear, though, is that these HEMTs are susceptible to SEB for fairly low LET ions and the use voltage for this particular version would have to be substantially derated to ensure reliable operation in space, if these early prototype parts were used without improvements. The test results for other layout versions (described below), however, shows a possible way to mitigate this problem.

Fig. 5 compares the data of Fig. 4, which were taken with a 5 μm G-D spacing, to those of other Type I devices with different G-D spacings, to look at the influence of this layout parameter. Due to time constraints, fewer devices with G-D variations were tested, so the data are more sparse for other types at this time, but we intend to remedy this with future testing.

这些hemt 在低let条件下对seb敏感，使用对这种特定情况下的电压可以有效降低seb来保证可靠的条件，如果原型期间没有经过提高的话。测试结果就会显示一个降低这种情况的结果对于其他测试结果。

This article has been accepted for publication in a future issue of this journal, but has not been fully edited. Content may change prior to final publication. Citation information: DOI 10.1109/TNS.2018.2885526, IEEE Transactions on Nuclear Science

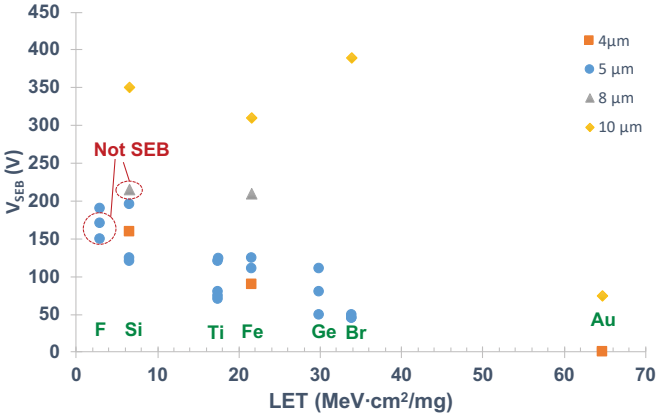

Figure 5: Plot of the minimum voltage for SEB for Type I HEMTs versus LET of the incident ions in the channel for different G-D spacings. The ion species are shown above their respective LETs for clarity. Three devices which failed for non-SEB breakdown are labeled as such, and are shown as unfilled points. Error bars not visible are smaller than marker. Each marker represents a single device, and all data are for normal incidence, with a test fluence of 2.5×10^7 ions/cm^2.

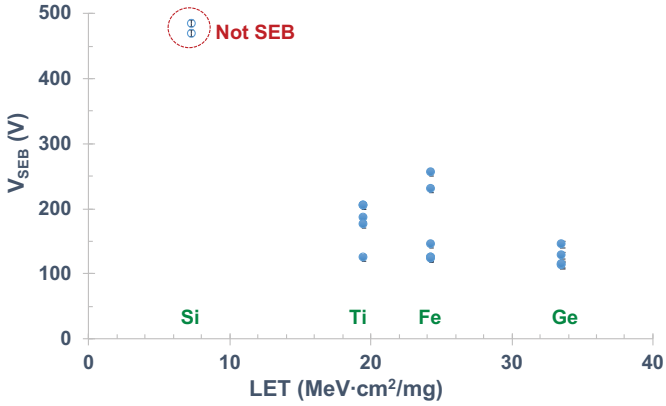

Figure 6: Plot of the minimum voltage for SEB for 500 V, Type II HEMTs versus LET of the incident ions in the channel. The ion species are shown above their respective LETs for clarity. Error bars not visible are smaller than marker. Each marker represents a single device, and all data are for normal incidence, with a test fluence of 2.5×10^7 ions/cm^2.

Either because of the lithography registration tolerance for the process (typically estimated as on the order of 1 µm, though visual inspection indicated very good alignment on our samples), or because of the relative size of the sensitive area to this difference, devices with G-D spacings of 4 µm and 5 µm had a very similar SEB response. The data for G-D spacing of 8 µm is sparse, with only one observed SEB event. Despite this, the result for Fe (21.6 MeV·cm^2/mg) indicates that the larger spacing can improve the SEB threshold, since its V_{SEB} is approximately the same as the BV_{DS} observed when trying to trigger SEB with Si ions. The data taken with a G-D spacing of 10 µm support this observation, as they show similar V_{SEB} up through Br (33.9 MeV·cm^2/mg), and possibly even heavier ions with higher LETs, though there is definitely a point where SEB does become a problem, since for Au (64.7 MeV·cm^2/mg), V_{SEB} is reduced to 87.5 V ± 12.5 V (i.e., the device passed at 75 V, but failed at 100 V, as described above). It would seem, then, that increasing the G-D spacing for the same device structure can mitigate the lowered SEB threshold in such devices. This is examined more in the following section on failure modes, mechanisms, and their implications.

The final group of heavy ion data to examine is for the other epitaxial structure, Type II, shown in Fig. 6. Layout dimensions are the same as the base Type I device, with G-D spacing of 5 µm, and nominal BV_{DS} is 500 V. Based on the limited amount of data that we currently have, it appears that these devices behave qualitatively like Type I devices of the same layout. The difference here is that BV_{DS} is much higher and the LET of most ions is also slightly higher. For Ge (33.6 MeV·cm^2/mg – almost identical to the LET of Br for Type I transistors) V_{SEB} is about 25% of BV_{DS}, as it was for Type I with Br ions. Also similar is the near immunity to SEB from Si (4.4 MeV·cm^2/mg).

The primary difference, in terms of SEB threshold, is that V_{SEB} appears to fall much more rapidly among the lower LET values than what is seen in Fig. 4. For example, with Ti (19.5 MeV·cm^2/mg) and Fe (24.3 MeV·cm^2/mg) ions, V_{SEB} is already less than 50% of BV_{DS}, which did not happen consistently for Type I until Br (33.9 MeV·cm^2/mg for the Type I), though it is still a secondary effect compared to the broader response. So, there appears to be an enhanced SEB sensitivity for Type II, beyond what would be expected from the slightly higher LET of ion species alone. We plan, in future work, to do similar tests for this structure with larger G-D spacing to see if a similar benefit is realized for Type II as for Type I.

B. Failure Modes, Mechanisms, and Implications

Following testing, all devices were photographed as part of a basic failure analysis. The images show the damage wrought by these catastrophic failures, but, more importantly, they show a distinct pattern that gives insight into the failure mechanism responsible. These insights are supported by the oscilloscope traces captured during burnout.

While the details of how the high currents and associated localized heating physically damaged them differ from one device to another, they share some key characteristics. The most important trait they share is a single spot bridging gate and drain, randomly located among the gate and drain fingers, which we hypothesize is the location of the heavy ion strike that caused SEB. An example showing this is in Fig. 7.

The area between gate and drain is the most obvious point for a failure to begin when a device is biased in the off state with a high drain voltage. In this state, the highest electric fields are in this area, with far lower fields (nearly two orders of magnitude in some cases) between gate and source. Our hypothesis is that a heavy ion strikes in the high-field region between gate and drain, and connects them, either directly through the created charge or by beginning impact ionization (avalanche) in the space. This hypothesis is supported by oscilloscope traces captured during burnout events, which show that the events begin with a simultaneous drop in drain voltage and sharp

提高间距可以提高seb阈值，因为vseb和bvds大致接近。

提高lgd可以提高seb的阈值电压

当高电流和局部加热结合起来的时候，伤害有所不同，有一些关键特征。最重要的共享的特征是一个单粒子连接栅和漏，随机的在栅极和漏的条形电极上，我们认为这个是重离子轰击导致的seb的位置。

栅极漏极之间的电场被入射粒子连接起来，不管是直接的或者是雪崩的。这个可以在烧毁过程中的轨迹捕获支持，证明事件是在漏电压的降低栅电压的升高开始。

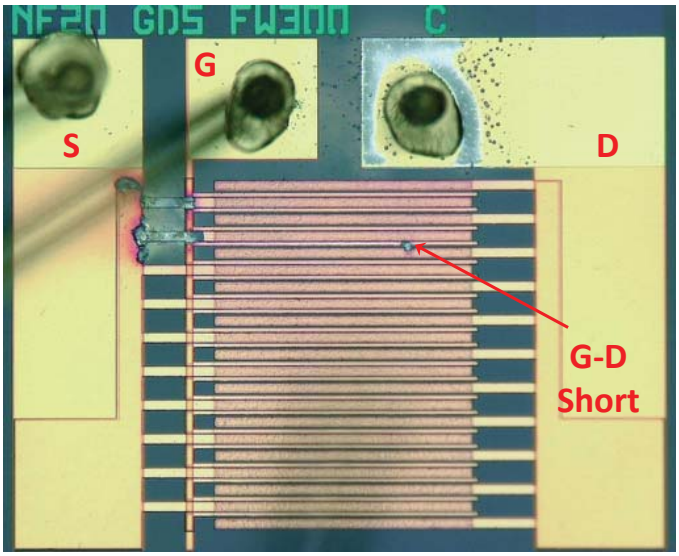

Figure 7: Photomicrograph showing typical device after SEB. Arrow indicates the site of G-D short that is believed to initiate the failure. Source, gate, and drain are labeled for clarity.

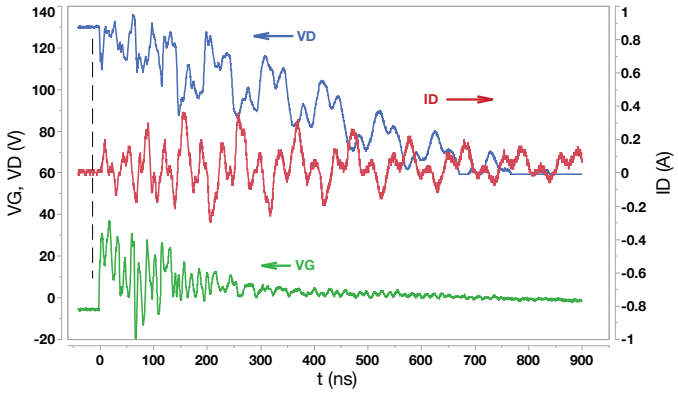

Figure 8: Example of a typical burnout transient captured on an oscilloscope. For this example, V_{DS}=130 V, V_{GS}=-6 V, the ion species was Fe, and the device type was Type II. Dashed vertical line marks the beginning of burnout, when the ion strikes. The slow decay in the drain voltage is attributed to the large capacitance between drain and ground, which provided charge for the SEB event. The high-frequency components are believed to be interactions between reactive circuit elements and device instability as it is turned on strongly.

increase in gate voltage. A sample of such a captured transient is shown in Fig. 8. The shape of the captured transients follow the general shape shown in Fig. 8, with no systematic variation that followed changes in drain bias (gate bias was fixed). The authors attempted to collect transient signals that were not destructive events to see what the evolution of the signals showed, but no signals above the noise floor were seen.

Examining the burnout transients shows several time constants. The most obvious is the long time constant for the drain voltage, which corresponds to the 1 µF drain capacitor discharging through a very low resistance (<10 Ω — approximately the on-resistance of a normal device). Superimposed on this is at least two other time constants that are much shorter. The longer of the two corresponds to about 10 MHz, and is present on most of the captured events, and we believe it is in an interaction of device instability (when the gate voltage goes high, the channel is turned on very strongly) and circuit parasitics. The shorter time constant is highly variable among the captured events, and is believed to be noise from the destructive processes. Note how drain current and drain voltage appear to trade between each other (drain voltage troughs align with drain current peaks), which we believe is evidence that drain current is partially shunting through the gate, as well as through the channel in this early stage (gate current was not recorded). Additional instrumentation in future tests should clarify this.

The behavior of the gate voltage is more straightforward. After the initial step up to over 35 V (in this example), there is high frequency ringing, and a much longer decay to ground, as physical damage to the device structure unfolds. Since the gate voltage never rises to the level of the drain voltage, it is clear that the connection between gate and drain is imperfect and very short-lived. As noted above, when the gate voltage goes high, the channel is suddenly very conductive, and offers an alternate path for current from the drain, which is still at a high potential.

Even as the gate voltage comes down, the channel remains on, since these are depletion-mode devices. Once the G-D connection happens, we can't describe the sequence of events with confidence (for instance, we don't know the role of conduction through the gate barrier layer and the channel). It is, however, clear from the damage to both drain and source connections, bond pads, and bond wires, that large currents are involved (drain currents of several amps were recorded in some cases) – well above those for which the devices were designed. In most cases, the crossover between gate metal and source metal lines also broke down, but it is impossible to tell when. The final state of devices was approximately evenly split between drains shorted to ground and open circuits, which appears to be dependent on the details of how the physical damage evolved during the event (e.g., currents high enough to fuse open bond wires result in an open circuit).

What we believe is most clear from failure analysis is our hypothesis that the destructive processes begin with a single ion strike between gate and drain which connects them, beginning a cascade of irreversible processes. (It should be noted that this mechanism is related, but not identical to, what is described in [4], and is distinct from mechanisms proposed in [2&3].) These processes can include dielectric breakdown in G-S metal crossovers, forward biasing of the gate-channel heterojunction, strong turn-on of the channel while a high bias is on the drain, and other effects, though the order is not known or entirely predictable, given the variety of gross damage patterns seen in this study. We believe that the lack of precursor transients at lower voltages is consistent with this hypothesis, in that at the threshold of SEB, an ion strike must be ideally placed, and deposit sufficient charge to bridge gate and drain. Any ion strike that does not meet both criteria will result in very little charge collection compared to the enormous changes that such an event triggers (particularly considering the thin layers normally available for collection), and would not be easily measured in this system. Irradiating at angles more perpendicular to gate and drain contacts, as in [4] would give useful information about the

时间最长的是漏电压，对应了漏电容通过一个特别小的电阻充电，接近开态电阻最长频率是10mhz, 时间最长是10-7

栅漏异常导通，栅源也异常导通，但不知道是什么时候。最后器件均匀的从漏到地剥离，开路。

单粒子导致栅漏短接，然后导致后续不可逆转的级联是确定的。比如介质击穿 栅极沟道异质结正向偏压，沟道在漏压高或者其他作用下强开启等，但是顺序不清楚。

高电压和瞬态前体是两个条件

栅极电压很高的时候沟道会导通，电势很高，即使栅极关断了仍然导通。

This article has been accepted for publication in a future issue of this journal, but has not been fully edited. Content may change prior to final publication. Citation information: DOI 10.1109/TNS.2018.2885526, IEEE Transactions on Nuclear Science

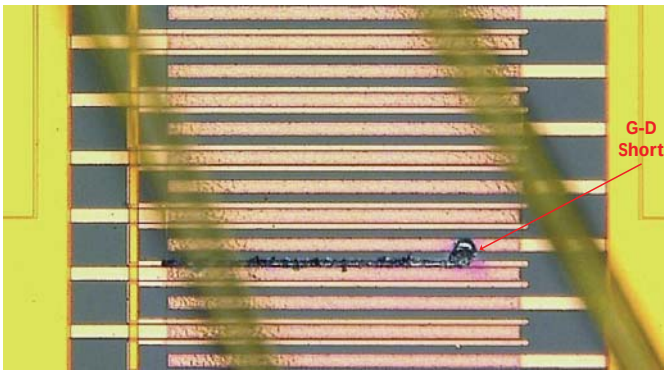

Figure 9: A photomicrograph showing detail of a Type I device with gate-drain spacing of 10 µm, after SEB event, with the characteristic connection between gate and drain.

safe operating area. A closer examination of the Type I devices with a larger gate-drain spacing, as shown in Fig. 9, supports this.

It is intuitively obvious that a larger spacing makes bridging the space more difficult. Fig. 5 showed the higher V_{SEB} for larger gate-drain spacing, L_{GD}, as expected, since BV_{DS} is higher. However, it also showed that, particularly for L_{GD}=10 µm, the large spacing permitted the devices to maintain the higher V_{SEB} for heavier ions, at least up to Br (33.9 MeV · cm^2/mg). This is illustrated more clearly in Fig. 10 and Fig. 11, which replot some of the data from Fig. 5 to show this. Fig. 10 shows the V_{SEB} data for only Si, Fe, and Br (in order of respective LETs) ions, but as a function of L_{GD}, clearly revealing the expected trend. The same data is replotted in Fig. 11 (with the L_{GD}=8 µm point removed for clarity) as a function of LET, which shows the other trend: for small L_{GD}, V_{SEB} decreases quickly with LET, while LET=10 µm shows no such decrease. We recommend that future work should explore this further by finding what value of L_{GD} shows no further improvement in robustness to ions with higher LET, improving the statistical basis for these findings, filling in more LET values, and examining the trade-offs with other device performance metrics.

未来的工作可以找到lgd的阈值，在更高的let条件下不变的值。

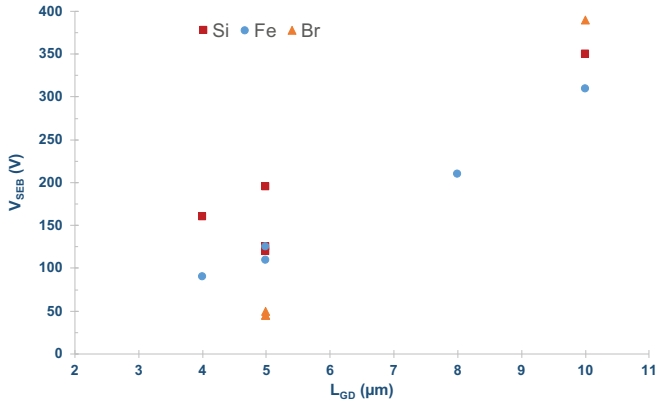

Fig. 10: Plot of V_{SEB} versus gate-drain spacing, L_{GD}, for Si, Fe, and Br ions, showing the dependence, and the reduction in V_{SEB} for heavier ions when L_{GD} is small.

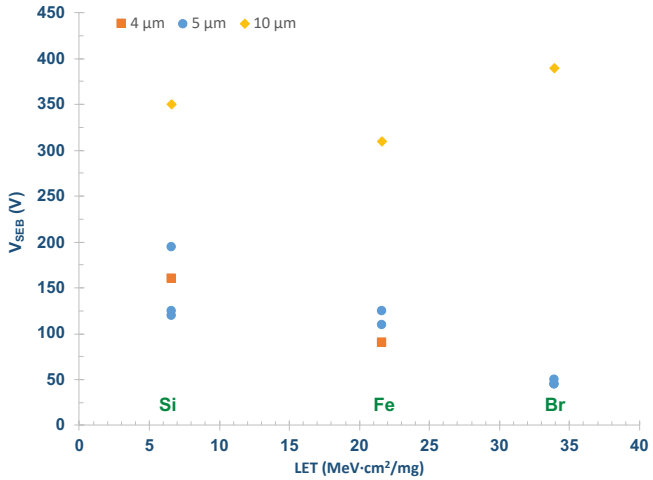

Fig. 11: Data of Fig. 10 plotted as a function of LET, showing the decline in V_{SEB} as LET increases for smaller L_{GD}, while for L_{GD}=10 µm keeps approximately the same V_{SEB} over this range. The point for L_{GD}=8 µm is not shown to enhance clarity.

C. *Proton Irradiation Effects*

Separate samples of Type I devices (L_{GD}=5 µm) were irradiated with 2.5 MeV protons at the Ion Beam Laboratory of Sandia National Laboratories, Albuquerque, NM. Devices were characterized before and after each exposure to protons in logarithmic steps of fluence. In the following figures, the total ionizing dose was estimated using SRIM [9], to be 131 Mrad($Al_{0.45}Ga_{0.55}N$) at the maximum fluence of 1×10^{14} p/cm^2. Fig. 12 shows drain current versus gate voltage from these exposures. (This type of irradiation has bulk, rather than localized effects, so it is not expected to have a different response from what is described below for different G-D spacings. Similarly, the higher Al content of Type II devices is not expected to change the trends described below, though there may be a small increase in the magnitude of the effects. These

相似的，更高的al组分可能有微小的提高，但是整体趋势是不可能变的，这个假说之前没有用实验研究证明过。

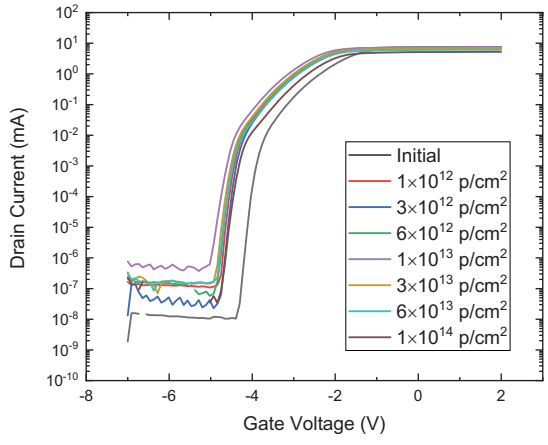

Figure 12: Plot of drain current versus gate voltage showing the example response to 2.5 MeV proton irradiation for a Type I device. Total ionizing dose was estimated to be 131 Mrad($Al_{0.45}Ga_{0.55}N$) at the maximum fluence of 1×10^{14} p/cm^2.

This article has been accepted for publication in a future issue of this journal, but has not been fully edited. Content may change prior to final publication. Citation information: DOI 10.1109/TNS.2018.2885526, IEEE Transactions on Nuclear Science

hypotheses, however, have not yet been explored experimentally.)

The data show a complex interplay of TID and DD. Following irradiation, devices show an initial increase in leakage current, simultaneous decrease in threshold voltage (V_{TH}), and increasing drive current (drain current for gate voltage above threshold) until a fluence of 1×10^{13} p/cm^2. Fig. 13 summarizes V_{TH} and $I_{DS,ON}$, where V_{TH} is the gate voltage at which drain-source current, I_{DS}, equals 1 μA for V_{DS}=2 V, and $I_{DS,ON}$ is I_{DS} for V_{GS}=2 V and V_{DS}=2 V. The initial device response to proton irradiation shows strong similarities to previous studies on AlGaN/GaN material systems [12]. The change in leakage and threshold voltage is most easily explained by net positive charge trapping [13]. Equivalently, the change in threshold voltage and leakage could be explained as the ionization of donor-like defect states in the bulk of the AlGaN buffer layer where the associated deep-levels act as a virtual potential that couples to the channel of the device. With increased proton irradiation, gradually, the introduction of defects within the bulk of the AlGaN layer is observed to cause a positive shift in threshold voltage, countering the initial net positive charge trapping process. This second process is explained by compensating negative charge trapping, likely due to the introduction of deep acceptor states that act to compensate the electron channel population. Acceptor-like traps also act as a source of scattering for transport processes resulting in increased on-state resistance. We note the high damage threshold of these materials is consistent with previous proton irradiation results on the GaN material system [12-15]. While defect introduction and device characteristics are *strongly* dependent on growth and fabrication conditions for AlGaN/GaN based devices, the native defects and radiation-induced defects of a high Al-mole fraction AlGaN material have been observed to exhibit many of the same deep-levels [16-19].

Fig. 14 shows the conventional drain transfer curves of a transistor for the same proton exposures. The changes in V_{TH} and the effects on $I_{DS,ON}$ are fairly evident both above and below the knee, respectively, for each gate voltage. We do note the relatively small change in $I_{DS,ON}$ under proton irradiation. We

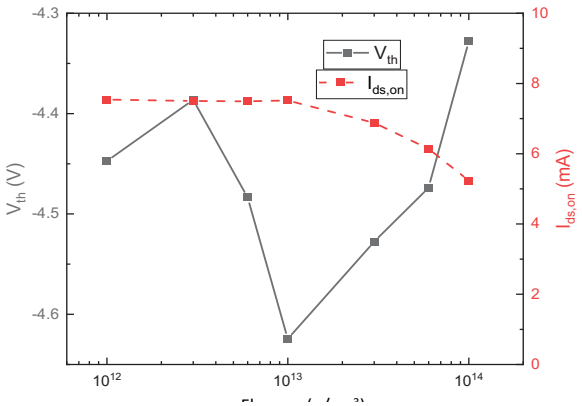

Figure 13: Summary plot of the data of Fig. 12, using the definitions of V_{TH} and $I_{DS,ON}$ described in the text. $I_{DS,ON}$ shows a steady decline as proton fluence increases and the more complex behavior of V_{TH}. This result is for a Type I device.

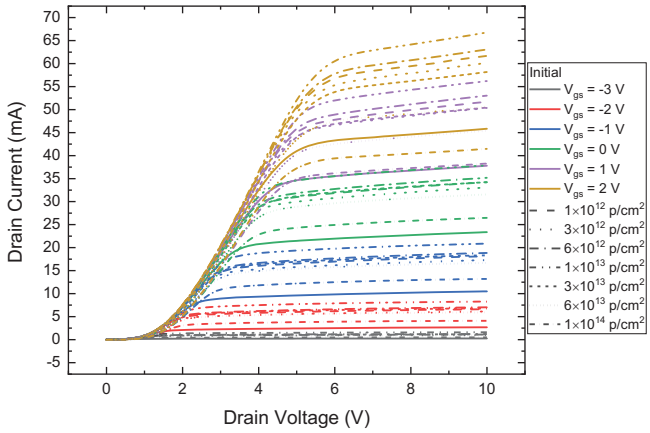

Figure 14: Drain transfer curves of an example transistor for various 2.5 MeV proton fluences. The effects on the saturated drain current are the most obvious result, though it is also possible to detect the changes to the channel resistance below the knee voltage.

note that the impact of proton irradiation on the device operating frequency is of great interest, as the channel resistance and introduction of electrically active deep-levels introduce potential τ=RC time constant penalties and will adversely affect device gain [20].

IV. Summary

This work has shown that research prototypes of AlGaN-based HEMTs have a reduced SEB threshold in simulated space environments such that design improvements would be needed to avoid significant derating of these types of devices for use in space applications. The data presented here suggest one could mitigate this lowered SEB threshold by increasing the G-D spacing, and optimizing SEB robustness and other performance metrics together as technology development goes forward. We hypothesize that these data show that burnout events begin with a heavy ion strike in the vulnerable region between gate and drain. This subsequently initiates a cascade of events resulting in damage that is largely manifested elsewhere in the device. This hypothesis is consistent with using G-D spacing as a tool in improving the overall robustness of these devices to SEB without the need for severe derating. While additional characterization testing is needed to more fully describe the trade-offs, we have shown that one can substantially improve the robustness of this technology for use in space environments. Proton exposures in this work show little reason for concern for TID and DD effects, which would be the other possible issue in space.

Acknowledgment

Special thanks to Chuck Carlson and the rest of the staff at the Tandem Van de Graff accelerator of Brookhaven National Laboratory for their help and support while testing there. Thanks to George Vizkelethy for help with proton irradiation. Thanks to Jeff Black, Paul Dodd, Nathan Nowlin, Will Rice, and Marty Shaneyfelt for their very helpful technical

discussions. Thanks to Mike Van Heukelom for help with electrical safety and test hardware.

V. References

[1] S. Kuboyama, A. Maru, H. Shindou, N. Ikeda, H. Abe, and T. Tamura, "Single-Event Damages Caused by Heavy Ions Observed in AlGaN/GaN HEMTs," *IEEE Trans. Nuc. Sci.,* vol. 58, *no.6*, pp. 2734-2738, Dec. 2011.

[2] M. Rostewitz, K. Hirche, J. Lätti and E. Jutzi, "Single Event Effect Analysis on DC and RF Operated AlGaN/GaN HEMTs," *IEEE Trans. Nuc. Sci.*, vol. 60, no. 4, pp. 2525-2529, Aug. 2013.

[3] L. Scheick, "Determination of Single-Event Effect Application Requirements for Enhancement Mode Gallium Nitride HEMTs for Use in Power Distribution Circuits," *IEEE Trans. Nuc. Sci.,* vol. 61, no. 6, pp. 2881-2888, Dec. 2014.

[4] E. Mizuta, S. Kuboyama, Y. Nakada, A. Takeyama, T. Ohshima, Y. Iwata, and K. Suzuki, "Single Event Damage Oserved in GaN-on-Si HEMTs for Power Control Applications," *IEEE Trans. Nuc. Sci.*, vol. 65, no. 8, pp. 1956-1963, Aug. 2018.

[5] R. J. Kaplar, A. A. Allerman, A. M. Armstrong, M. H. Crawford, J. R. Dickerson, A. J. Fischer, A. G. Baca, and E.A. Douglas, "Review—Ultra-Wide-Bandgap AlGaN Power Electronic Devices," *ECS J. Solid State Sci. and Tech.*, vol. 6, no. 2, pp. Q3061-3066, Dec. 2017.

[6] A. G. Baca, A. A. Armstrong, A. A. Allerman, B. A. Klein, E.A. Douglas, C. A. Sanchez, and T. R. Fortune, "High Temperature Operation of $Al_{0.45}Ga_{0.55}N/Al_{0.30}Ga_{0.70}N$ High Electron Mobility Transistors," *ECS J. Solid State Sci. and Tech.*, vol. 6, no. 11, pp. S3010- S3013, Aug. 2017.

[7] A. G. Baca, B. A. Klein, A. A. Allerman, A. M. Armstrong, E. A. Douglas, C. A. Stephenson, T. R. Fortune, and R. J. Kaplar, "$Al_{0.85}Ga_{0.15}N/Al_{0.70}Ga_{0.30}N$ High Electron Mobility Transistors with Schottky Gates and Large On/Off Current Ratio over Temperature," *ECS J. Solid State Sci. and Tech.*, vol. 6, no. 12, pp. Q161- Q165, Dec. 2017.

[8] S. Bazzoli, S. Girard, V. Ferlet-Cavrois, J. Baggio, P. Paillet and O. Duhamel, "SEE sensitivity of a COTS GaN transistor and silicon MOSFETs," *2007 9th European Conference on Radiation and Its Effects on Components and Systems*, Deauville, France, September 10-14, 2007, pp. 1-5.

[9] J.F. Ziegler, The Stopping and Range of Ions in Matter, 2012 [Online], Available http://www.srim.org.

[10] A. E. Waskiewicz, J. W. Groninger, V. H. Strahan and D. M. Long, "Burnout of Power MOS Transistors with Heavy Ions of Californium-252," *IEEE Trans. on Nuc. Sci.*, vol. 33, no. 6, pp. 1710-1713, Dec. 1986.

[11] R.A. Medwalt, "Elemental Composition and Energy Spectra of Galactic Cosmic Rays, *Proc. Conf. on Interplanetary Particle Environment*, JPL Publication 88-28, pp. 121-132, JPL, Pasadena, CA, April 15, 1988.

[12] J. Chen, Y. S. Puzyrev, C. X. Zhang, E. X. Zhang, M. W. McCurdy, D. M. Fleetwood, R. D. Schrimpf, S. T. Pantelides, S. W. Kuan, E. C. H. Kyle, and J. S. Speck, "Proton-induced dehydrogenation of defects in AlGaN/GaN HEMTs," *IEEE Trans. on Nuc. Sci.*, vol. 60, no. 6, pp. 4080-4086, Dec. 2013.

[13] M. P. King A. M. Armstrong, J. R. Dickerson, G. Vizkelethy, R. M. Fleming, J. Campbell, W. R. Wampler, I. C. Kizilyalli, D. P. Bour, O. Aktas, H. Nie, D. Disney, J. Wierer, A. A. Allerman, M. W. Moseley, F. Leonard, A. A. Talin, and R. J. Kaplar, "Performance and Breakdown Characteristics of Irradiated Vertical Power GaN P-i-N Diodes," *IEEE Trans. on Nuc. Sci.*, vol. 62, no. 6, pp. 2912-2918, Dec. 2015.

[14] J. Chen, Y. Z. Puzyrev, R. Jiang, E. X. Zhang, M. W. McCurdy, D. M. Fleetwood, R. D. Schrimpf, S. T. Pantelides, A. R. Arehart, S. A. Ringel, P. Saunier, and C. Lee, "Effects of Applied Bias and High Field Stress on the Radiation Response of GaN/AlGaN HEMTs," *IEEE Trans. on Nuc. Sci.*, vol. 62, no. 6, pp. 2423-2430, Dec. 2015.

[15] Y. Z. Puzyrev, T. Roy, E. X. Zhang, D. M. Fleetwood, R. D. Schrimpf, and S. T. Pantelides, "Radiation-Induced Defect Evolution and Electrical Degradation of AlGaN/GaN High-Electron-Mobility Transistors," *IEEE Trans. on Nuc. Sci.*, vol. 58, no. 6, pp. 2918-2924, Dec. 2011.

[16] A. Y. Polyakov, M. Shin, J. A. Freitas, M. Skowronski, D. W. Greve, and R. G. Wilson, "On the Origin of Electrically Active Defects in AlGaN Alloys Grown by Organometallic Vapor Phase Epitaxy," *J. Appl. Phys.*, vol. 80, No. 11, pp. 6349-6354, Dec. 1996.

[17] A. Y. Polyakov, N. B. Smirnov, A. V. Govorkov, E. A. Kozhukhova, S. J. Pearton, F. Ren, L. Liu, J. W. Johnson, W. Lim, N. G. Kolin, S. S. Veryovkin, and V. S. Ermakov, "Comparison of Neutron Irradiation Effects in AlGaN/AlN/GaN, AlGaN/GaN, and InAlN/GaN Heterojunctions," *J. Vac. Sci. Technol. B*, vol. 30, Issue 6, 061207, Nov. 2012.

[18] A. Y. Polyakov, S. J. Pearton, P. Fenzer, F. Ren, J. Liu, and J. Kim, "Radiation Effects in GaN Materials and Devices," *J. Mater. Chem. C*, vol. 1, Issue 5, pp. 877-887, Feb. 2013.

[19] S. J. Pearton, R. Deist, F. Ren, L. Liu, A. Y. Polyakov, and J. Kim, "Review of Radiation Damage in GaN-based Materials and Devices," *J. Vac. Sci. Technol. A*, vol. 31, Issue 5, 050801, Sept. 2013.

[20] N.E. Ives, J. Chen., A. F. Witulski, R. D. Schrimpf, D. M. Fleetwood, R. W. Bruce, M. W. McCurdy, E. X. Zhang, and L. W. Massengill, "Effects of Proton-Induced Displacement Damage on Gallium Nitride HEMTs in RF Power Amplifier Applications," *IEEE Trans. on Nuc. Sci.*, vol. 62, no. 6, pp. 2417-2422, Dec. 2015.